

Kinetic-energy-release distributions and barrier heights for C_2^+ emission from multiply charged C_{60} and C_{70} fullerenes

N. Haag, Z. Berényi, P. Reinhed, D. Fischer, M. Gudmundsson, H. A. B. Johansson, H. T. Schmidt, and H. Cederquist
Department of Physics, Stockholm University, AlbaNova University Center, S-10691 Stockholm, Sweden

H. Zettergren

Department of Physics and Astronomy, University of Aarhus, DK-8000 Aarhus C, Denmark

(Received 24 July 2008; published 31 October 2008)

We present experimental kinetic-energy-release distributions in the asymmetric fission processes $C_{60}^{q+} \rightarrow C_{58}^{(q-1)+} + C_2^+$ and $C_{70}^{q+} \rightarrow C_{68}^{(q-1)+} + C_2^+$ for highly excited mother ions in charge states $q=4-8$. We find that the distributions for C_{70}^{q+} are considerably narrower and peak at lower energies than for C_{60}^{q+} in the corresponding charge state when $q > 4$. Further, semiempirical values for C_2^+ fission barrier heights were extracted for $q=4-6$ by means of a statistical approach and the measured intensity ratios between fission and C_2 evaporation.

DOI: 10.1103/PhysRevA.78.043201

PACS number(s): 36.40.Qv, 34.70.+e

I. INTRODUCTION

A vast number of collision studies involving fullerenes have been performed (see, e.g., Refs. [1,2] and references therein). Typical issues then concerned electron- and energy-transfer processes, fragmentation of fullerene ions with and without charge separation, and interrelations between these phenomena. Further, it has been realized that fullerenes may also serve as excellent model systems for radiation damage (fragmentation) studies of much less regular biomolecular systems (cf. [3,4]). When fullerenes collide with slow highly charged atomic ions several electrons may be transferred, to leave behind multiply ionized and, sometimes, intact fullerenes. Collisionally excited fullerene cations in charge states q up to 10 have been observed [5,6] with highly charged ions as projectiles, while the theoretically predicted stability limits are $q=14$ and 17 for C_{60} and C_{70} in their ground states, respectively [7,8].

Recently, Martin *et al.* [9] demonstrated by direct decay-channel-selective measurements of the energy deposition that the competition between different fullerene fragmentation channels depends on the charge state and the total internal excitation energy. This study, which relies on the population of single bound states in negative ions, also confirmed that excitation energies of the order of 40 eV or above are needed for C_2 emission on typical experimental time scales of microseconds [10]. In general, however, these internal excitation energies cannot be readily determined, at least not in experiments with highly charged ions, for which it often has been assumed that internal excitation energies mostly are much lower due to large impact parameters for multiple electron transfer [11–14].

Kinetic-energy-release distributions (KERDs) in unimolecular fragmentation processes may possibly provide valuable and so far missing information on the electron and energy transfer mechanisms, as their positions and shapes are governed by the potential-energy surfaces describing the interactions of the separating fragments in the exit channel. In the case of neutral C_2 evaporation,

$$C_n^{q+} \rightarrow C_{n-2}^{q+} + C_2 \quad (n = 60, 70), \quad (1)$$

kinetic-energy-release distributions have been measured earlier [15–17]. On the other hand, much less is known about the C_2^+ emission process (asymmetric fission)

$$C_n^{q+} \rightarrow C_{n-2}^{(q-1)+} + C_2^+ \quad (n = 60, 70). \quad (2)$$

A single experimental KERD for asymmetric fission has been reported by Senn *et al.* [18] in 1998, but the more recent results [6,19] are given as single (typical) values only. There are also no theoretical studies that could suggest a functional form for the KERD of (2). The processes (1) and (2) are most likely independent processes, well separated in time from the collision and controlled by activation energies and fission barriers, respectively [19–21]. For low q ($q \leq 4$), evaporation is normally the dominant fragmentation process, while first asymmetric fission and then multifragmentation (breakup into several small charged fragments) takes over as q increases [13,22]. The latter process is even more important in high-energy, heavy-ion, collisions where many electrons may be removed and large energies deposited in close collisions with the fullerenes [23].

In this work, we present a systematic study of experimental KERDs for asymmetric fission (2) of C_{60}^{q+} and C_{70}^{q+} with $q=4-8$. Somewhat to our surprise, we find that the KERDs for asymmetric fission from C_{60}^{q+} are considerably wider and have larger most likely values than the C_{70}^{q+} distributions in the corresponding charge states. The present results will be discussed together with recent theoretical results [7] and in view of the different properties of multiply charged C_{60} and C_{70} ions including their overall sizes, shapes, charge distributions, isomers, and vibrational modes. Further, we use the measured branching ratios between (1) and (2) and a statistical approach to deduce semiempirical values for the fission barrier heights which are in excellent agreement with high-level transition state calculations for C_{60}^{q+} [7].

II. EXPERIMENT

For the present study, we have developed a linear recoil-ion-momentum spectrometer which has been optimized for

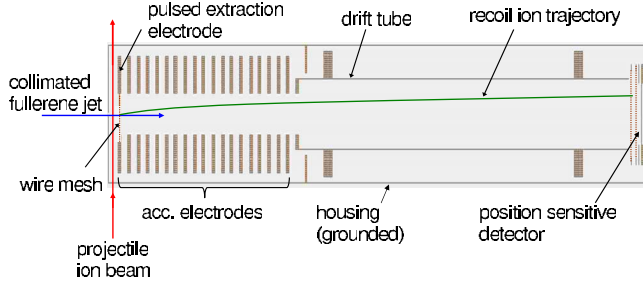


FIG. 1. (Color online) Schematic of the experimental setup.

measurements of KERDs for fragmenting complex molecules such as fullerenes or biomolecules. The spectrometer (see, Fig. 1) consists of an acceleration region with 19 ring electrodes in a grounded housing with a small aperture for the collinear target jet, a field-free drift region, and a position-sensitive detector with two microchannel plates (MCPs), 40 mm in diameter and a resistive anode. The dimensions of the spectrometer are chosen such that first-order time focusing for different trajectory starting points is achieved, i.e., the field-free drift region is twice as long as the distance between the beam-jet crossing and the end of the acceleration region. The ring electrode closest to the interaction region is covered with a wire mesh and connected to a separate voltage supply for pulsed extraction. Together with the 18 remaining ring electrodes, which are connected to a common dc-voltage supply through a resistor chain inside the vacuum, we define homogeneous acceleration fields of 6.0 and 9.0 V/mm.

Fullerene target jets are produced in a temperature-regulated sublimation oven (600 °C), which is carefully cleaned before changes between powders of C_{60} (Hoechst, purity 99.9%) and C_{70} (MER Corp., purity >99%). After collimation, the target jet enters the spectrometer along its axis where it crosses a pulsed (2 kHz, 5 μ s pulse length) beam of 57 keV Xe^{19+} ions ($v=0.4$ a.u.) from a 14.5 GHz electron cyclotron resonance ion source. An electrode at a constant potential of +20 V in front of the last jet-collimation aperture prevents positive ions from the fullerene oven (at ground potential) to reach the interaction region.

Intact ionized fullerenes and charged fragments are extracted toward the detector directly after the passage of the ion beam pulse by the negative extraction voltage pulse (100 μ s long) on the first ring electrode. The ion flight times, as deduced from the time differences between the extraction pulses and signals from the MCP, and the corresponding four anode corner signals yielding the position on the detector are stored in list mode on an event-by-event basis. The time of flight may be converted to the ions' mass-to-charge ratios, resulting in a spectrum like the one shown in Fig. 2 for the C_{60} target.

In Fig. 3, we show a series of detector images for multiply charged C_{58} fragments (left column) and multiply charged C_{68} fragments (right column), identified through their time of flight. Such two-dimensional distributions have contributions from both types of processes—evaporation of one neutral C_2 unit [Eq. (1)] from a mother ion in the same charge state, and asymmetric fission, i.e., emission of one C_2^+ ion [Eq. (2)] from a mother ion in the next higher charge state. The evapo-

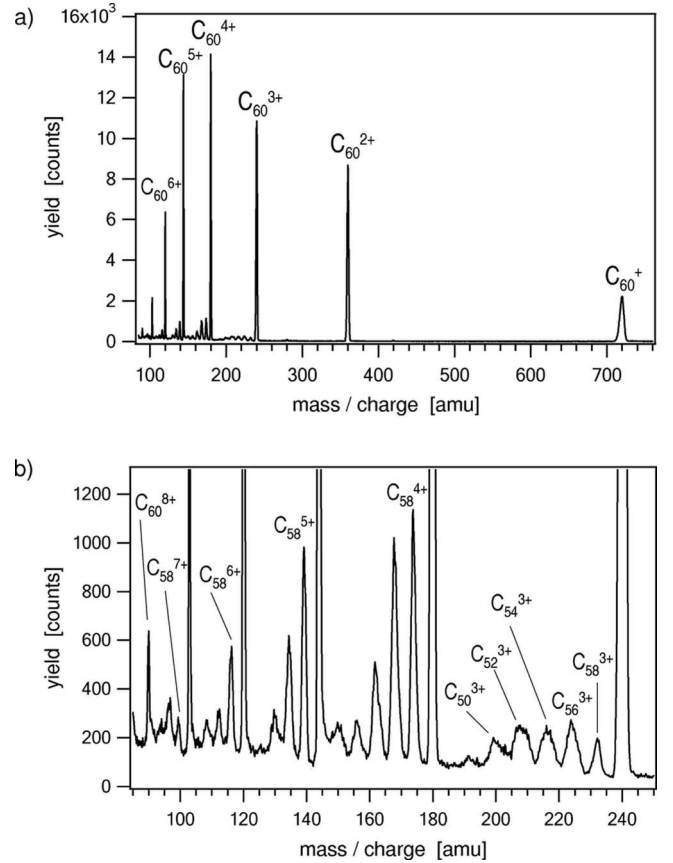


FIG. 2. Mass-to-charge ratio spectrum of ionized C_{60} and charged fragments produced in collisions with 57 keV Xe^{19+} . In (a), the full spectrum is shown with labels on the most prominent intact peaks. In (b), a zoom-in on the multiply charged heavy fragments is displayed (the intensities of most of the intact peaks are out of range).

ration processes mostly contribute to the spots close to the detector center due to the small KER values (typically a few tenths of an eV [24]). Fragments from the fission processes, however, have much wider position distributions as kinetic energy releases for two *charged* separating fragments range from a few eV up to several tens of eV as will be shown below. The (total) kinetic energy release, ϵ , is partitioned on both fragments but can be calculated from the kinetic energy (in the center-of-mass frame) of one fragment through momentum and energy conservation for two-body breakup.

III. DATA ANALYSIS

For, e.g., a C_{58} or a C_{68} fragment, the radial displacement r (in mm) from the spectrometer axis is

$$r = 4\kappa \sqrt{\frac{E_{\text{kin}}L}{3q'|\vec{E}|}} \sin \vartheta + r_0 \delta. \quad (3)$$

Here, E_{kin} is the kinetic energy in the laboratory frame in eV, $L=592$ mm is the distance from the beam-jet crossing to the detector, q' is the charge state of the fragment ion in atomic units, $|\vec{E}|$ is the acceleration field strength in V/mm, ϑ is the

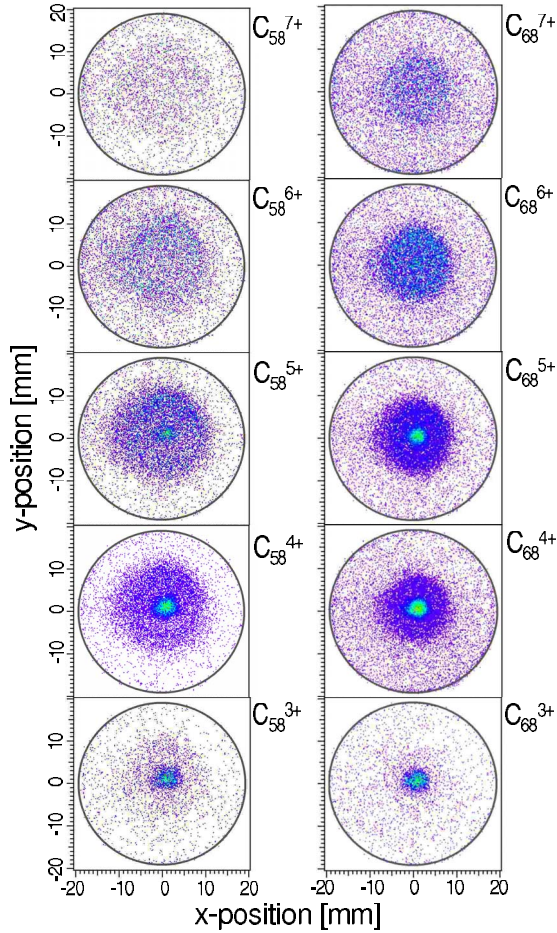


FIG. 3. (Color online) Two-dimensional detector images for multiply charged C_{58} (left column) and C_{68} ions (right column) due to fragmentation of C_{60} and C_{70} mother ions, respectively (see text).

angle between the ion velocity vector and the spectrometer axis, and r_0 (in mm) is the distance from this axis before extraction. The parameters κ and δ are corrections due to lens action in the fringe field between the acceleration and drift regions. For $\kappa=1$ and $\delta=1$, Eq. (3) describes the ideal case of a spectrometer without such a lens effect. In our case, the values are obtained through SIMION 7.0 simulations yielding $\kappa=1.274$ and (the magnification) $\delta=0.944$. In the following, we will use these values and perform simulations of the radial distributions of the heavy fragments ($C_{58}^{q' +}$ and $C_{68}^{q' +}$), taking into account the actual initial conditions and the time delay between fragmentation and extraction.

The initial velocity and spatial distributions of the neutral fullerene molecules before ionization were calculated from the known thermal distribution of fullerenes in the oven, the angular distribution of the effusive beam (following Ref. [25] and using the present actual oven-nozzle geometry), the jet collimation, and the finite volume of the overlap between the fullerene jet and the ion beam. Measurements and simulations of the radial distributions for the *intact* (i.e., nonfragmented) fullerene ions confirmed these calculations on a level appropriate for the present experiment. In this step, and in the following simulations of fragment energy distributions, we have assumed that recoil energies from the electron

transfer process may be neglected due to large impact parameters, short interaction times, and large target masses. We further assume that the fission and evaporation processes are isotropic in the rest frame of the mother ion, as the present fragmentation processes (the time scale ranges up to the order of microseconds) are slow in relation to the collision and fullerene rotations.

Two-dimensional detector images are simulated independently as functions of assumed probability distributions of the kinetic energy releases for evaporation, $P_e(\epsilon)$, and fission, $P_f(\epsilon)$, and are subsequently converted to radial distributions. Under real experimental conditions, there is an almost uniform background on the detector, which is accounted for by a radial background intensity linear in r . For the different assumed analytical forms of the KERDs, the simulated total radial distributions are fitted to those obtained from the experiment by nonlinear regression. Data from the two different acceleration field settings (6.0 and 9.0 V/mm) are fitted together. Finally, the $(P_e(\epsilon), P_f(\epsilon))$ combinations that give the best fit to our measured radial distributions are taken to be the present semiempirical results.

For the evaporation distributions we use the “model-free” approach by Klots [26]:

$$P(\epsilon) = a\epsilon^l \exp\left(-l\frac{\epsilon}{\tilde{\epsilon}}\right), \quad (4)$$

where a is a normalization factor, $\tilde{\epsilon}$ is the position of the maximum of the distribution, i.e., the most probable KER value, and l is a parameter related to the interaction potential between the separating fragments ($0 \leq l \leq 1$). Equation (4) has been used earlier to fit evaporation KERDs [16,17,24]. Following Głuch *et al.* [16] and Climen *et al.* [17], we take $l=0.5$ for the evaporation KERD, corresponding to a Langevin-like long-range interaction between C_2 and the heavier, charged fragment. This interaction potential scales with the center-center distance d between the two fragments as d^{-4} due to polarization effects.

For fission, the reverse activation barrier and the dynamics of the separation of charged products lead to difficulties in establishing proper theoretical descriptions [27]. As mentioned above, there are no theoretical studies of KER *distributions* for asymmetric fission and we have tried various assumptions for $P_f(\epsilon)$, like simply shifting a KERD similar to those for evaporation by the amount of the reverse activation barrier. This could not describe the experimental data, which was also the case for a symmetric, bell-shaped distribution, like, for example, the ones obtained with the maximum entropy method for specific reactions with a reverse barrier without charge separation [28,29].

In a first tentative effort to describe the present fission data we again use Eq. (4). The overall best fits to our experimental data are then obtained with $l=8.5$ (C_{60}) and $l=10.0$ (C_{70}) but for the moment we refrain from an attempt to interpret these results and only regard the resulting functions $P_f(\epsilon)$ as efficient ways to parametrize the experimental data. In this context we note that the only previously published KERD for fullerene fission, by Senn *et al.* [18] for C_{60}^{3+} fragmentation, also is well described by Eq. (4) with

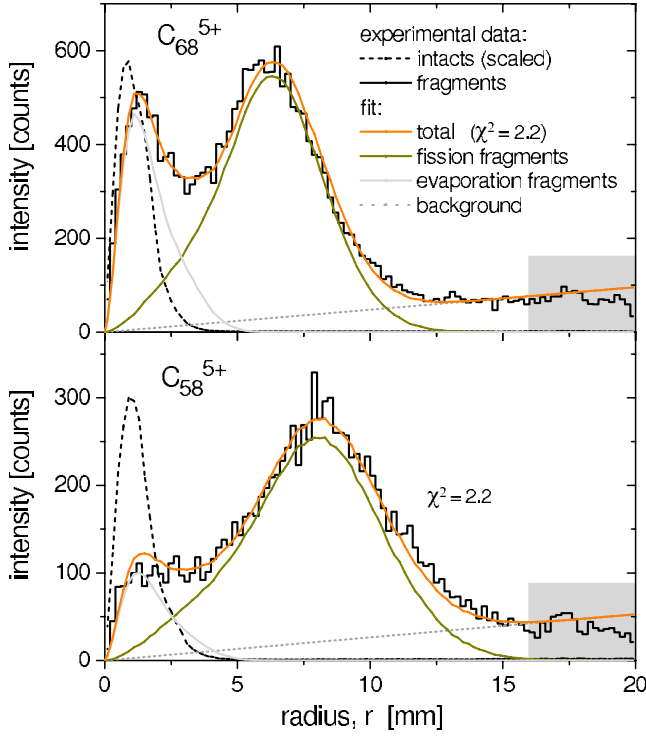


FIG. 4. (Color online) Experimental radial distributions of C_{58}^{5+} (lower panel) and C_{68}^{5+} (upper panel) with simulated and fitted distributions. Here, C_{60}^{5+} (C_{70}^{5+}) ions decaying via neutral C_2 evaporation give rise to the peaks at smaller radii. Fragments originating from C_2^+ emission from C_{60}^{6+} , or C_{70}^{6+} , respectively, contribute with broader peaks at larger radii. The background is assumed to be uniform (intensity linear in r) up to $r=16$ mm (see text). The radial distributions of intact C_{60}^{5+} (C_{70}^{5+}) ions are indicated by dashed lines (not to scale).

$l=8.5$. This result [18] was obtained with a different type of ionizing collision (electron impact) and a different experimental technique, the mass-analyzed ion kinetic energy (MIKE) technique, in which an electrostatic energy analyzer voltage is scanned to give the kinetic energy distribution of a preselected fragment from a given decay process.

In Fig. 4, the experimental and fitted radial distributions

are shown for C_{58}^{5+} and C_{68}^{5+} . The fit parameters are $\tilde{\epsilon}_f$ and $\tilde{\epsilon}_e$, the ratios between the intensities for fission and evaporation and the background intensity. Similar fits were made also for the other charge states. Events with $r > 16$ mm (shaded area in Fig. 4) are disregarded as the images are not perfectly centered on the detector. The reduced χ^2 values for the fits in Fig. 4 are $\chi^2=2.2$ in both cases, and between 1.2 and 2.6, and between 1.3 and 3.9 for the other charge states of C_{68} and C_{58} , respectively.

IV. RESULTS AND DISCUSSIONS

A. Kinetic-energy-release distributions

The fission KERDs $P_f(\epsilon)$ yielding the best fit results are presented in Fig. 5. For both C_{60}^{q+} and C_{70}^{q+} the width of the distributions increases with q . We find that the KERDs for $C_{60}^{4+} \rightarrow C_{58}^{3+} + C_2^+$ and $C_{70}^{4+} \rightarrow C_{68}^{3+} + C_2^+$ are very similar (see the left panel of Fig. 5). For higher charge states q of the mother ions, however, the distributions for C_{70} are narrower and shifted toward lower energies.

The total internal energy (after completion of electron transfer processes) E^* should be quite small for the majority of mother ions (large impact parameters), but may also range up to several tens of eV or above [9,30]. It is usually assumed that the electronic excitation energy is efficiently converted to vibrational energy. Very recently, Rentenier *et al.* [31] concluded that, in the specific case of the $He^{2+} + C_{60}$ system, such high excitation may be due to electron capture from inner π orbitals producing electronically excited fullerene ions also at large impact parameters. However, such excitation mechanisms are typical for projectiles of lower charge states for which densities of electron capture states on the projectile are limited. Electronic excitation of the fullerene ion might also be due to close collisions [32], but at the moment the mechanisms behind the substantial excitation that some of the multiply ionized fullerenes obviously obtain during the electron transfer process (which basically are dominated by large impact parameters) are not clear. In any case, the highly excited fullerene ions may decay by emission of a C_2^+ or a C_2 unit within the present experimental time frame of a few μs when a sufficiently large energy (B_f

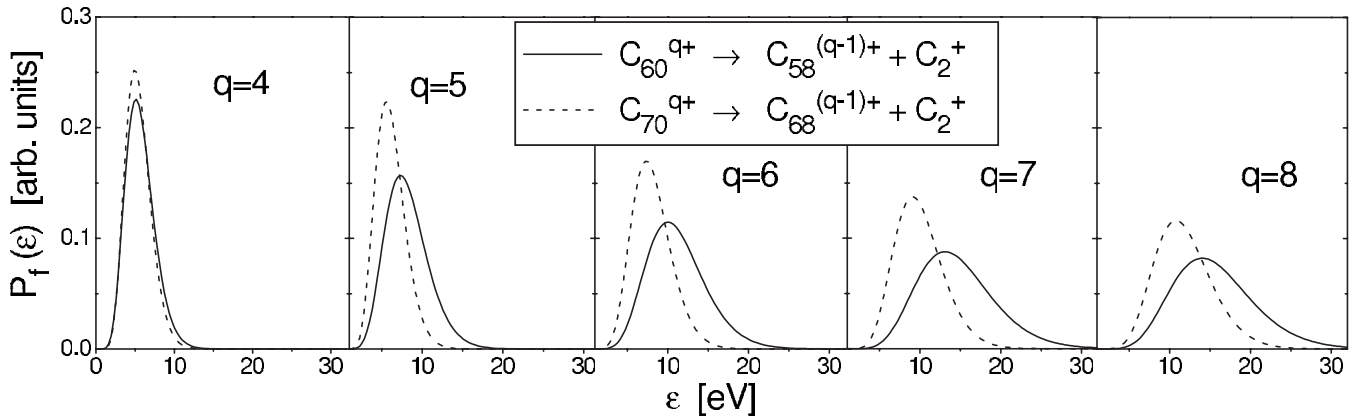


FIG. 5. Kinetic-energy-release distributions in asymmetric fission reactions of multiply charged C_{60} (solid curves) and C_{70} (dashed curves), as functions of charge state q . The distributions shown are optimized to reproduce the experimental data in the simulation and fit procedure described in the text.

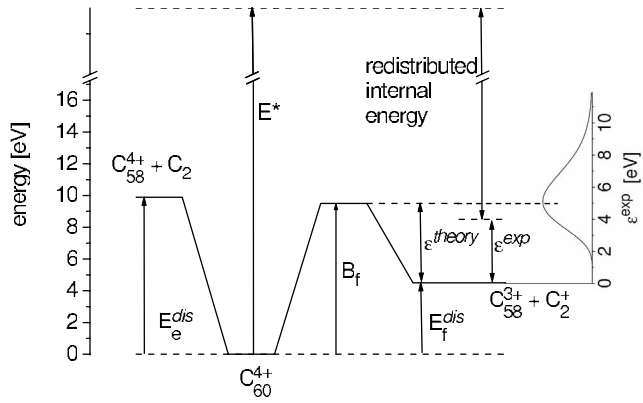


FIG. 6. Schematic of the two different decay channels and possible ways of partitioning the excess energy in the asymmetric fission reaction. The zero of the energy scale is the ground state of the mother ion. E_e^{dis} and E_f^{dis} denote the dissociation energies for C_2 and C_2^+ emission, respectively. B_f is the fission barrier height, and E^* is the total initial excitation energy of the mother ion. To the right: the present experimental KER distribution.

or E_e^{dis} , respectively) is concentrated in a particular dissociative mode. A schematic description of the competition between evaporation and fission is depicted in Fig. 6.

The fission process (2) proceeds through a transition state [7], for which the reverse activation barrier (equal to ϵ^{theory} in Fig. 6) would always be released as kinetic energy if the reaction coordinate were completely separated from the other modes. However, a non-negligible coupling of the reaction coordinate to the other rovibrational modes may lead to a situation in which the reverse activation barrier may partially be transformed to internal energy. Such a scenario is mindful of the one observed for the fragmentation of multiply charged fullerene dimers [33,34] in two intact, charged, monomers, where it was found that only about 50% of the potential energy at the equilibrium dimer distance was released as kinetic energy. The rest was converted to internal energy of the fullerenes. As can be seen in Fig. 6, where we show the present KERDs for asymmetric fission of C_{60}^{4+} (to the right), we also measure KER values higher than ϵ^{theory} . This may possibly be due to the existence of several local minima and transition states with different (higher) energies in the electronic ground state [21,35] (not shown in the simplified picture of Fig. 6). Another explanation could be that the high ϵ values are due to transition states related to remaining nonthermalized electronically excited states as discussed by Chen *et al.* [30]. The presently observed increases of distribution widths with q appear to be linked to increases (with q) of the reverse activation barrier heights.

The measured differences in the kinetic energy releases for C_{60}^{q+} and C_{70}^{q+} may be attributed to differences in molecular properties like polarizability, size, and shape— C_{60} is spherical while C_{70} is not. A further aspect, which may be important, is the less homogeneous charge distribution on C_{70} ions compared to C_{60} . Zettergren *et al.* [36] found that multiply charged C_{70} fullerenes have some essentially neutral bonds (the central bonds in the pyrene motifs) regardless of the charge state. The larger C_{70} molecule, and the C_{68} product, also have higher numbers of vibrational degrees of

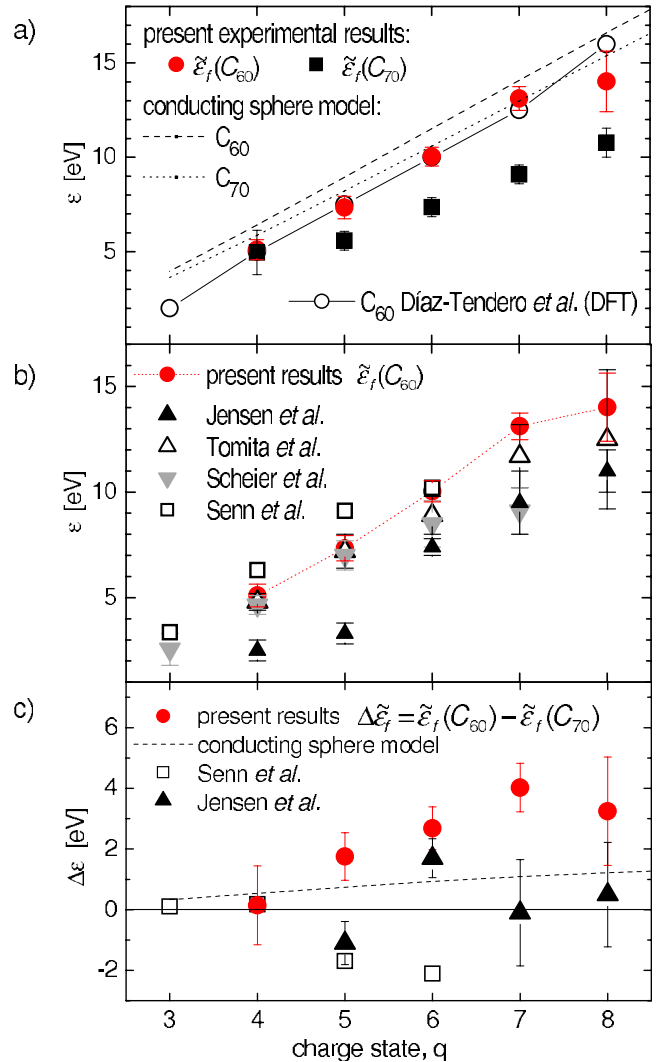


FIG. 7. (Color online) Comparison of the present most probable KER values for asymmetric fission of C_{60}^{q+} and C_{70}^{q+} with (a) results from DFT calculations [7] (with lines to guide the eye) and an electrostatic model [6,38]; (b) other experiments on C_{60} yielding single typical values by Scheier *et al.* [39], Tomita *et al.* [19], Senn *et al.* [18], and Jensen *et al.* [6]. (c) The difference between the $\tilde{\epsilon}_f$ values for C_{60}^{q+} and C_{70}^{q+} .

freedom which possibly may favor that more energy is kept as internal energy in the fragmentation process than for the C_{60} case. In forming C_{68} products we probably also effectively have higher fission dissociation energies, E_f^{dis} , in comparison to what we would get if the lowest C_{68} isomer were formed. There are many more isomers for C_{68} than for C_{58} , and such effects would give lower reverse barriers resulting in lower measured kinetic-energy releases. Finally, it has been suggested [37] that isotopic effects (it is more likely to find one or several ^{13}C atoms in C_{70} than in C_{60}) and related anharmonic behavior may account for the observed differences between C_{60} and C_{70} .

In Fig. 7, the most probable values of our kinetic-energy-release distributions for fission of C_{60}^{q+} and C_{70}^{q+} , $\tilde{\epsilon}_f$, are shown as functions of q . In the case of C_{60} , these values agree almost perfectly with high level density functional

theory (DFT) transition state calculations [7] [see Fig. 7(a) in which the DFT results of [7] are connected by solid lines]. The theoretical values are for the molecules in their ground states only (cf. Fig. 6) and do not include excitations, de-excitations, or possible isomeric transformations during the separation process. It is thus surprising, and perhaps also to some extent fortuitous, that the agreement between experiment and the transition state calculations of [7] is so good in the case of C_{60} .

There are several earlier measurements of kinetic energy releases for fission from multiply charged fullerenes, but with the exception of [18] they report only “typical values” and not the full distributions. Comparing our results for C_{60} to such single-valued KER results [Fig. 7(b)], we note that our most likely values are in agreement with the results of Tomita *et al.* [19] for $q=4-8$. The results by Scheier *et al.* [39], obtained with the MIKE technique, also agree with the present ones except for their highest charge state ($q=7$). The same technique was used also by Senn *et al.* [18], who, however, report values significantly above the present results, except for $q=6$, whereas the results by Jensen *et al.* [6] are significantly lower in all cases. The technique used by Jensen *et al.* [6] was similar to the present one but was not fully optimized for measurements of details in the KERDs due to smaller detector images and much larger spectrometer fringe fields. Further, the results in Ref. [6] for $q=4$ and 5 are much too low due to unresolved contributions from evaporation. Taking the differences between most likely ϵ values for C_{60} and C_{70} , $\Delta\tilde{\epsilon}_f = \tilde{\epsilon}_f(C_{60}) - \tilde{\epsilon}_f(C_{70})$, we find that the present results follow a trend *opposite* to the one by Senn *et al.* [18], whereas the data by Jensen *et al.* [6] do not show a clear trend at all [see Fig. 7(c)]. The observed difference has a similar behavior as a function of q as a simple electrostatic model [6,38] but is a factor of 2-3 larger than the model prediction. The model takes the different polarizabilities of C_{60} and C_{70} due to their overall difference in size into account but ignores the fact that C_{70} is not spherical and has a less homogeneous charge distribution than C_{60} .

The most probable KER values for evaporation, $\tilde{\epsilon}_e$, are measured to range between approximately 70 and 80 meV for $q=4-6$. For $q>6$, the evaporation yield was too small to contribute significantly to the total experimental radial distribution. This is about 50% smaller than values reported from MIKE experiments [16]. However, the present experiment is optimized for the much larger ϵ values in the fission processes (2). Thus, detector images for evaporation are very small.

B. Branching ratios and fission barrier heights

In Table I we show the present experimental fission branching ratios, obtained from the fits and defined as the number of mother ions of a given charge state q decaying by emission of one (and only one) C_2^+ unit, divided by the total number of mother ions decaying via emission of either one C_2^+ or one C_2 . Branching ratios deviating significantly from zero and 100% are observed for $q=4-6$. For C_{70} these ratios are lower than for C_{60} in the corresponding charge states. As the branching ratio is very sensitive to the difference be-

TABLE I. Experimental branching ratio (in percentage) for fission (C_2^+ emission) relative to evaporation (C_2 emission) as obtained by the fits of the radial intensity distributions (see text). The statistical errors are about ± 1.0 .

	Charge state q		
	4	5	6
C_{60}^{q+}	18.9	87.5	98.2
C_{70}^{q+}	4.8	64.5	96.1

tween fission barrier height (B_f) and the dissociation energy for evaporation (E_e^{dis}), we tentatively use a simple statistical model to extract semiempirical values for the fission barrier heights for $q=4-6$. Here we rely on theoretical E_e^{dis} values (considering the most stable isomers) for $C_{60/70}^{q+} \rightarrow C_{58/68}^{q+} + C_2$ from Díaz-Tendero *et al.* [21] and Zettergren *et al.* [8], whereas the fission barriers are free fit parameters. This is a reasonable approach since it is much easier to calculate E_e^{dis} than B_f , which requires calculation of the transition states.

We use classical Rice-Ramsperger-Kassel theory [40,41] and for ionized C_n ($n=60,70$) fullerenes with a total excitation energy E^* distributed on the vibronic degrees of freedom (see Fig. 6), the probability of locating at least the energy B_f in one of the $s=3n-6$ modes is $(1-B_f/E^*)^{s-1}$. Hence, the rate constants for fission and evaporation, k_f and k_e , become [40,41]

$$k_f = \begin{cases} g_f A (1 - B_f/E^*)^{s-1} & \text{if } E^* \geq B_f, \\ 0 & \text{if } E^* < B_f, \end{cases} \quad (5)$$

$$k_e = \begin{cases} g_e A (1 - E_e^{\text{dis}}/E^*)^{s-1} & \text{if } E^* \geq E_e^{\text{dis}}, \\ 0 & \text{if } E^* < E_e^{\text{dis}}, \end{cases} \quad (6)$$

where A is a common frequency factor and g_e and g_f are degeneracy factors. Here, we use the recent results on evaporation from singly charged fullerenes by Concina *et al.* [42]: $A=1.2 \times 10^{21} \text{ s}^{-1}$ for C_{60} and $8.5 \times 10^{19} \text{ s}^{-1}$ for C_{70} . Further, as there is no independent information on fission frequency factors in the literature, we assume that the values are the same as for evaporation.

In the case of C_{60} ions, the q positive charges are equally “distributed” on all 90 bonds but it is the removal of one of the 60 C_2 units shared by a hexagon and a pentagon that leads to the most stable C_{58} isomers [21]. For evaporation from C_{60} ions we thus take $g_e=60-(60/90)q$, and for fission we assume $g_f=(60/90)q$. For the less symmetric C_{70} case there are many more isomers and possible transformations involved, resulting in a larger number of ways to remove a C_2 unit, and the most stable multiply charged C_{68} isomer, referred to as C_2 -I in Ref. [8], can only be reached indirectly, i.e., by isomerization. In order to estimate the reaction degeneracy, we therefore consider the lowest C_{68} isomer that can be formed *directly* by C_2 or C_2^+ extraction from a C_{70}^{q+} isomer. In Ref. [43] this C_{68} geometry, which is about 0.3 eV higher in energy than C_2 -I [8], is referred to as C_s (SW), and the type of bonds in the C_{70} associated with its formation are

labeled SW1 and SW2 (due to the preceding Stone-Wales transformation [44]). There are 20 such bonds and we assume that the charge is equally distributed on all 105 bonds in C_{70} except for the central bonds in the five pyrene motifs, which are not charged [36]. Thus, we assume $g_e=20-[20/(105-5)]q$ for evaporation and $g_f=[20/(105-5)]q$ for fission.

Assuming exponential decay, the probability for decay within the time τ is

$$\rho = 1 - e^{-(k_e+k_f)\tau} = \rho_e + \rho_f, \quad (7)$$

where

$$\rho_e = [k_e/(k_e + k_f)]\rho \quad (8)$$

and

$$\rho_f = [k_f/(k_e + k_f)]\rho \quad (9)$$

are the probabilities for decay via evaporation and fission, respectively. Note that ρ , k_e , k_f , ρ_e , and ρ_f are functions of E^* . Here, we have used $\tau=3 \mu\text{s}$, which is the average time between ionization and extraction in the experiment (5- μs -long ion beam pulses and a short delay between the end of the pulse and extraction). We neglect the influence from decay processes during acceleration and drift in the field-free region of the spectrometer, which, for the case of C_{60}^{3+} and $|\vec{E}|=6 \text{ V/mm}$, takes about $25 \mu\text{s}$. This is, to some extent, supported by the absence of significant tails on the peaks in the time-of-flight spectra.

After single C_2^+ or C_2 emission, the C_{58} and C_{68} fragments may still be highly excited and, therefore, we also take the possibility of subsequent decay within $\tau=3 \mu\text{s}$ into account. This gives changes in shapes and decreases of integral intensities of ρ_e and ρ_f . In this second step, the internal energies of the C_{58} and C_{68} fragments are reduced by $(E_e^{\text{dis}} + \epsilon)$ or $(E_f^{\text{dis}} + \epsilon)$ from E^* and we use $A=2 \times 10^{19} \text{ s}^{-1}$ for both C_{58} and C_{68} [42]. Finally, the fission ratios R are determined through

$$R = \frac{\int \rho_f dE^*}{\int (\rho_f + \rho_e) dE^*}, \quad (10)$$

where ρ_e and ρ_f now are the probabilities for emitting just one C_2 or just one C_2^+ , respectively. As the same internal energy range contributes to both processes (see Fig. 8 for an example), the actual distributions of initial excitation energies E^* , which are not exactly known for the present experiment, hardly affect the ratio R . Further, R is insensitive to the absolute value of the A factors and to changes in τ on the level of a few microseconds.

For each q , the fission barrier height, and thus k_f , was adjusted such that R agrees with the experimental result in Table I. The semiempirical B_f values are shown in Fig. 9 with estimated uncertainties. Our results for C_{60} are in agreement with high-level DFT transition state calculations [7]. This very favorable comparison is a bit surprising given the simplicity of the present statistical approach. The B_f values obtained for C_{70} are lower than the theoretical results by Zettergren *et al.* [8], which, however, are based on the assumption of equal reverse barriers for C_{60} and C_{70} . Thus, the

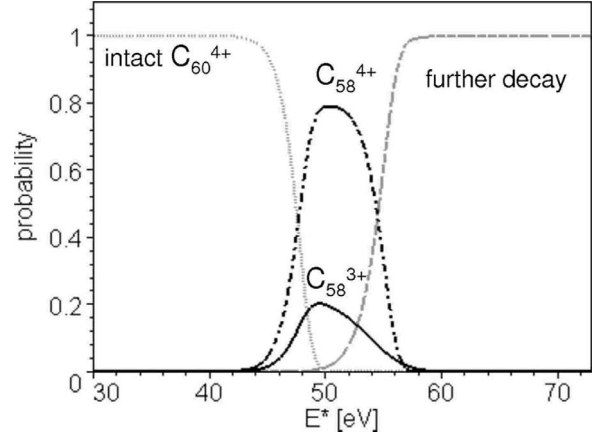


FIG. 8. Modeled probabilities for C_{60}^{4+} mother ions with internal excitation energy E^* to stay intact (dotted gray curve), decay via emission of one C_2 (dash-dotted black curve), or one C_2^+ (solid black curve), or further decay to smaller fragments (gray dashed curve) within $\tau=3 \mu\text{s}$.

results in Fig. 9 indicating lower fission barriers for C_{70} than for C_{60} are in principle consistent with the present measurements of smaller kinetic energy releases for C_{70} , although the differences in B_f values in Fig. 9 are too small to fully explain the observation.

V. CONCLUSION

In this work, we have presented a systematic experimental study of kinetic-energy-release distributions for single C_2^+ emission from multiply charged C_{60} and C_{70} fullerenes (in charge states $q=4-8$). Further, based on measured branching ratios between C_2 and C_2^+ emission and a simple statistical approach, we have deduced semiempirical fission barrier heights for C_{60} and C_{70} ions in charge states $q=4-6$. We find large, unexpected differences between the KERDs for C_{60} and C_{70} , where the former are wider and peak at significantly larger values when $q>4$. We believe that the lower C_{70} fission barriers, the larger C_{70} polarizability (size), and the fact

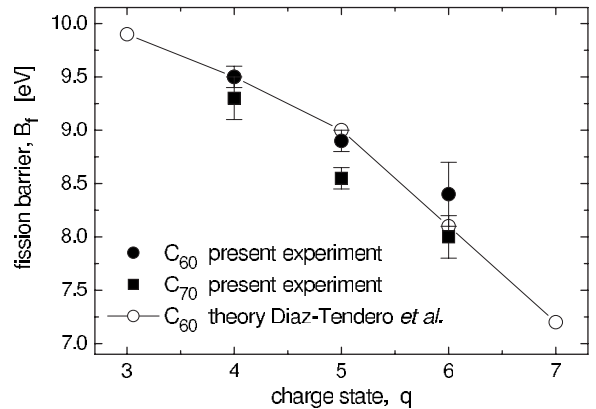


FIG. 9. Semiempirical fission barriers with estimated errors for C_{60}^{q+} (filled circles) and C_{70}^{q+} (filled squares). Results for C_{60}^{q+} from theory (DFT) [7] are shown by open symbols and are connected by lines to guide the eye.

that it is likely that the ground state C_{68} isomer is *not* formed in C_{70} fragmentation contribute to this difference, although they do not fully explain it. Additional effects may concern the inhomogeneous charge distribution on C_{70} , its nonspherical shape, and isotope effects. The peak positions of the present KERDs for C_{60} coincide with high-level transition state calculations for ground state fragments by Díaz-Tendero *et al.* [7] and, further, our semiempirical fission barrier heights agree perfectly with the results from the same calculation. The wide experimental distributions show that kinetic energy releases may be both smaller and larger than the reverse activation barrier. The lower energies may be explained as due to couplings of the reaction coordinate with other internal degrees of freedom, while the larger values possibly may relate to higher-lying transition states for the

electronic ground state or remaining electronic excitations with larger reverse barriers. Our experiment and analysis again shows that substantial internal excitation energies—of the order of 50 eV or above—are involved in fragmentation of fullerene ions on the microsecond time scale. At the moment, the mechanism behind this substantial excitation is not clear and this intriguing and very important problem needs to be studied in further detail.

ACKNOWLEDGMENTS

We are grateful to Patrik Löfgren and Mikael Blom at the Manne Siegbahn Laboratory for their help in preparing the ion beam. The support by the European Project ITS LEIF (Grant No. RII3/026015) is gratefully acknowledged.

-
- [1] E. E. B. Campbell and F. Rohmund, *Rep. Prog. Phys.* **63**, 1061 (2000).
- [2] E. E. B. Campbell, *Fullerene Collision Reactions* (Kluwer Academic, Dordrecht, 2003).
- [3] B. Liu, S. Brøndsted Nielsen, P. Hvelplund, H. Zettergren, H. Cederquist, B. Manil, and B. A. Huber, *Phys. Rev. Lett.* **97**, 133401 (2006).
- [4] B. Liu, N. Haag, H. Johansson, H. T. Schmidt, H. Cederquist, S. Brøndsted Nielsen, H. Zettergren, P. Hvelplund, B. Manil, and B. A. Huber, *J. Chem. Phys.* **128**, 075102 (2008).
- [5] A. Brenac, F. Chandezon, H. Lebius, A. Pesnelle, S. Tomita, and B. A. Huber, *Phys. Scr.*, T **80B**, 195 (1999).
- [6] J. Jensen, H. Zettergren, H. T. Schmidt, H. Cederquist, S. Tomita, S. B. Nielsen, J. Rangama, P. Hvelplund, B. Manil, and B. A. Huber, *Phys. Rev. A* **69**, 053203 (2004).
- [7] S. Díaz-Tendero, M. Alcamí, and F. Martín, *Phys. Rev. Lett.* **95**, 013401 (2005).
- [8] H. Zettergren, G. Sánchez, S. Díaz-Tendero, M. Alcamí, and F. Martín, *J. Chem. Phys.* **127**, 104308 (2007).
- [9] S. Martin, L. Chen, A. Salmoun, B. Li, J. Bernard, and R. Brédy, *Phys. Rev. A* **77**, 043201 (2008).
- [10] R. Wörgötter, B. Dünser, P. Scheier, T. D. Märk, M. Foltin, C. E. Klots, J. Laskin, and C. Lifshitz, *J. Chem. Phys.* **104**, 1225 (1996).
- [11] B. Walch, C. L. Cocke, R. Voelpel, and E. Salzborn, *Phys. Rev. Lett.* **72**, 1439 (1994).
- [12] J. Jin, H. Khemliche, M. H. Prior, and Z. Xie, *Phys. Rev. A* **53**, 615 (1996).
- [13] S. Martin, L. Chen, A. Denis, R. Bredy, J. Bernard, and J. Désesquelles, *Phys. Rev. A* **62**, 022707 (2000).
- [14] H. Cederquist *et al.*, *Phys. Rev. A* **61**, 022712 (2000).
- [15] S. Matt, O. Echt, M. Sonderegger, R. David, P. Scheier, J. Laskin, C. Lifshitz, and T. D. Märk, *Chem. Phys. Lett.* **303**, 379 (1999).
- [16] K. Gluch, S. Matt-Leubner, O. Echt, R. Deng, J. U. Andersen, P. Scheier, and T. D. Märk, *Chem. Phys. Lett.* **385**, 449 (2004).
- [17] B. Climen, B. Concina, M. A. Lebeault, F. Lépine, B. Bague-nard, and C. Bordas, *Chem. Phys. Lett.* **437**, 17 (2007).
- [18] G. Senn, T. D. Märk, and P. Scheier, *J. Chem. Phys.* **108**, 990 (1998).
- [19] S. Tomita, H. Lebius, A. Brenac, F. Chandezon, and B. A. Huber, *Phys. Rev. A* **67**, 063204 (2003).
- [20] H. Cederquist, J. Jensen, H. T. Schmidt, H. Zettergren, S. Tomita, B. A. Huber, and B. Manil, *Phys. Rev. A* **67**, 062719 (2003).
- [21] S. Díaz-Tendero, M. Alcamí, and F. Martín, *J. Chem. Phys.* **123**, 184306 (2005).
- [22] S. Martin, L. Chen, A. Denis, and J. Désesquelles, *Phys. Rev. A* **57**, 4518 (1998).
- [23] T. LeBrun, H. G. Berry, S. Cheng, R. W. Dunford, H. Esbensen, D. S. Gemmell, E. P. Kanter, and W. Bauer, *Phys. Rev. Lett.* **72**, 3965 (1994).
- [24] S. Matt, M. Sonderegger, R. David, O. Echt, P. Scheier, J. Laskin, C. Lifshitz, and T. D. Märk, *Int. J. Mass. Spectrom.* **185/186/187**, 813 (1999).
- [25] W. Steckelmacher, R. Strong, and M. W. Lucas, *J. Phys. D* **11**, 1553 (1978).
- [26] C. E. Klots, *Z. Phys. D: At., Mol. Clusters* **21**, 335 (1991).
- [27] J. Laskin and C. Lifshitz, *J. Mass Spectrom.* **36**, 459 (2001).
- [28] D. Fati, A. J. Lorquet, R. Loch, J. C. Lorquet, and B. Leyh, *J. Phys. Chem. A* **108**, 9777 (2004).
- [29] E. Gridelet, D. Dehareng, R. Loch, A. J. Lorquet, J. C. Lorquet, and B. Leyh, *J. Phys. Chem. A* **109**, 8225 (2005).
- [30] L. Chen, S. Martin, J. Bernard, and R. Brédy, *Phys. Rev. Lett.* **98**, 193401 (2007).
- [31] A. Rentenier *et al.*, *Phys. Rev. Lett.* **100**, 183401 (2008).
- [32] J. Opitz, H. Lebius, B. Saint, S. Jacquet, B. A. Huber, and H. Cederquist, *Phys. Rev. A* **59**, 3562 (1999).
- [33] H. Zettergren, H. T. Schmidt, P. Reinherd, H. Cederquist, J. Jensen, P. Hvelplund, S. Tomita, B. Manil, J. Rangama, and B. A. Huber, *Phys. Rev. A* **75**, 051201(R) (2007).
- [34] H. Zettergren, H. T. Schmidt, P. Reinherd, H. Cederquist, J. Jensen, P. Hvelplund, S. Tomita, B. Manil, J. Rangama, and B. A. Huber, *J. Chem. Phys.* **126**, 224303 (2007).
- [35] R. L. Murry, D. Strout, G. K. Odom, and G. E. Scuseria, *Nature (London)* **366**, 665 (1993).
- [36] H. Zettergren, M. Alcamí, and F. Martín, *ChemPhysChem* **9**, 861 (2008).
- [37] P. Scheier (private communication).

- [38] H. Zettergren, H. T. Schmidt, H. Cederquist, J. Jensen, S. Tomita, P. Hvelplund, H. Lebius, and B. A. Huber, *Phys. Rev. A* **66**, 032710 (2002).
- [39] P. Scheier, B. Dünser, and T. D. Märk, *Phys. Rev. Lett.* **74**, 3368 (1995).
- [40] O. K. Rice and H. C. Ramsperger, *J. Am. Chem. Soc.* **49**, 1617 (1927).
- [41] L. S. Kassel, *J. Phys. Chem.* **32**, 225 (1928).
- [42] B. Concina, S. Tomita, J. U. Andersen, and P. Hvelplund, *Eur. Phys. J. D* **34**, 191 (2005).
- [43] W. C. Eckhoff and G. E. Scuseria, *Chem. Phys. Lett.* **216**, 399 (1993).
- [44] A. J. Stone and D. J. Wales, *Chem. Phys. Lett.* **128**, 501 (1986).